Water Science & Technology

Water Science & Technology Vol 84 No 9, 2265 doi: 10.2166/wst.2021.446

Synthesis and characterization of arginine-doped heliotrope leaves with high clean-up capacity for crystal violet dye from aqueous media

Lahoucine Brini[a,*], Abdelghani Hsini[b], Yassine Naciri[b], Asmae Bouziani[c], Zeeshan Ajmal[d], Khalihana H'Maida[a], Aziz Boulahya[a], Mohamed Arahou[a], Bahcine Bakiz[b], Abdallah Albourine[b] and Mohammed Fekhaoui[a]

[a] Laboratory of Animal Zoology and Ecology, Scientific Institute, Mohammed V University, Rabat, Morocco
[b] Laboratory of Materials and Environment, Faculty of Sciences, Ibn Zohr University, Agadir, Morocco
[c] Chemical Engineering Department, Middle East Technical University, Ankara, Turkey
[d] College of Engineering, China Agricultural University, Beijing 100083, China
*Corresponding author. E-mail: brini.houcine@gmail.com

AB, 0000-0001-6045-3608; BB, 0000-0001-6457-8424

ABSTRACT

A novel arginine-modified Heliotrope leaf (Arg@HL) was used as adsorbent for the crystal violet (CV) dye adsorption in a batch process. The physicochemical and morphological composition of Arg@HL were characterized by field-emission scanning electron microscopy (FE-SEM), Fourier transform infrared (FTIR) spectroscopy, thermogravimetric analysis (TGA), and differential scanning calorimetry (DSC). The experiments were carried out to investigate the factors that influence the dye uptake by the adsorbent, such as the contact time under agitation, adsorbent amount, initial dye concentration, temperature and pH of dye solution. The optimum conditions of adsorption were found on the batch scale as followed: CV concentration of 20 mg·L^{-1}, an amount of 0.75 g·L^{-1} of the adsorbent, 90 min contact time, 6 pH and 25 °C temperature for Arg@HL. The results confirmed a second-order model explaining the dye crystal violet's adsorption's kinetics by Arg-Heliotrope leaves. The Langmuir model effectively defines the adsorption isotherms. The results revealed that the Arg@HL has the potential to be used as a low-cost adsorbent for the removal of CV dye from aqueous solutions.

Key words: adsorption, Arg-Heliotrope leaves, arginine, isotherm, kinetics, thermodynamic

HIGHLIGHTS

- The first effort to use a low-cost arginine-modified Heliotrope leaves material as an adsorbent for crystal dye elimination by adsorption procedures.
- CV dye was efficiently removed using Arg@HL.
- Arg@HL exhibited high adsorption capacity for CV dye.
- Adsorption process follows the Langmuir isotherm.

1. INTRODUCTION

In the last decades, the pollution of water by organic and inorganic chemical pollutants has become a major public worry (Chennah *et al.* 2018, 2019; Hsini *et al.* 2020a, 2020b; Abdellaoui *et al.* 2021; Ajmal *et al.* 2021; Laabd *et al.* 2022). Dyes are pollutants that can be seen by the naked eye (Essekri *et al.* 2020; Ferraa *et al.* 2020). They are utilized in different industries like elastic, plastics, and beauty care products (Fegousse *et al.* 2019). Besides, colored chemicals in the aquatic environment lead to a considerable reduction in light transmittance and the amount of dissolved oxygen in water, thereby affecting the plant photosynthesis activity (Essekri *et al.* 2020). Moreover, synthetic dyes are well known as stable and complex biodegradable compounds, which promote their accumulation in aquatic ecosystems (Essekri *et al.* 2020). Over 7×10^5 tones and 10,000 different types of dyes and pigments are produced worldwide annually. Crystal violet dye is widely used in textile manufactories for dyeing cotton and silk and also in the manufacturing of paints and printing inks (Sulyman 2014). Therefore, the industrial dye-containing effluents should be adequately handled before their release into the environment.

The advancement of a viable economic method of waste management for the coloring industry has long been essential for protecting the environment. In order to clean wastewater and eliminate dyes, numerous treatment approaches have been employed, like photodegradation (Ait Ahsaine *et al.* 2018; Naciri *et al.* 2018, 2019a, 2019b, 2020a, 2020b, 2021; Chennah *et al.* 2019; Erdogan *et al.* 2019; Shaim *et al.* 2019; Barebita *et al.* 2020; Bouziani *et al.* 2020, 2021; Akhsassi *et al.* 2021; Mimouni *et al.* 2021), biological oxidation (Paz *et al.* 2017; Sathishkumar *et al.* 2019), nanofiltration membranes (Saffaj *et al.* 2005), ozonation (Oguz *et al.* 2005; Gharbani *et al.* 2008), and adsorption (Kizito *et al.* 2017a, 2017b; Ajmal *et al.* 2018, 2020a, 2020b; Aarab *et al.* 2020a, 2020b; Ba Mohammed *et al.* 2020). The latter is enhanced compared to other wastewater treatment methods in terms of its preliminary expense, flexibility, easiness of layout, ease of function, and insensitivity toward toxic pollutants (Benafqir *et al.* 2019; Hsini *et al.* 2020a, 2021a, 2021b).

Activated carbon (AC) is considered the oldest and commonly utilized adsorbent for wastewater purification (Naushad *et al.* 2019a, 2019b; Hasanzadeh *et al.* 2020). AC has a high adsorption capacity and rate; however, its high cost is a significant drawback for its utilization (Garg *et al.* 2004). For this purpose, numerous tries have been conducted to study dyes' adsorption via low-cost and organic adsorbents such as natural agro-industrial or plant waste materials (Tunç *et al.* 2009; Mittal *et al.* 2010; Mahmood *et al.* 2017).

Fallen leaves of heliotrope are in ample supply, cheap, and readily accessible in numerous Morocco regions. These leaves have no use in the commercial field and are not consumed by livestock. There are no earlier published articles on the usage of these leaves for eliminating dyes from aqueous solutions. Hence, the heliotrope leaves as a low-cost and ample bio-sorbent could be an alternate for the removal of dyes from wastewater.

L-arginine (Arg) is amino acid which has good prospects to bind with cations through electrostatic force over a wide pH range. The Arg is widely used to modify the substrate surface to prepare a high-performing adsorbent (Hsini *et al.* 2020a). Thus, it can be anticipated that leaves of heliotrope modified with arginine would have a strong affinity with cationic CV dye and could be efficiently used to remove CV dye under specific conditions.

Until today, no systematic research on chemical functionalization (by L-arginine (Arg)) of leaves of heliotrope as an adsorbent for wastewater treatment has been described. Hence, the main objective of this research was to discover the possibility of Arg@HL as an inexpensive natural and non-conventional adsorbent for CV dye uptake from its aqueous solution. The effect of initial dye concentration, initial solution pH, contact time, adsorbent dose, and temperature on CV dye adsorption were studied. Moreover, this article also presented different thermodynamic parameters such as Gibbs free energy change (ΔG^0), heat of adsorption (ΔH^0), and entropy change (ΔS^0). On the other hand, the Arg@HL's textural properties and surface chemistry are also characterized extensively.

2. MATERIALS AND METHOD

2.1. Synthesis of Arg-heliotrope leaves

The Arginine surface functionalization of heliotrope leaves was carried out according to the following procedure: 20 g of heliotrope leaves (HL) powder was dispersed in 400 ml of 0.1M NaOH solution and stirred for two hours. Then, the mix was filtered and rinsed several times until the filtrate solution attained a neutral pH. The obtained material was dried at 50 °C for 12 h. Afterward, 10 g of HL treated by NaOH were mixed with 100 ml of 0.6 M Arginine solution followed by stirring for two hours. The mixture was thermally processed at 120 °C in an oven for 90 min. Finally, the obtained HL functionalized by Arginine (labeled Arg@HL) was rinsed numerous times with distilled water, then dried at 60 °C for six hours.

2.2. Arg-heliotrope leaves characterization

A JEOL, JSM-IT200 scanning electron microscope (SEM) was utilized to analyze the synthesized samples' morphology. Fourier-transform infrared (FTIR) (wavenumber from 400 to 4,000 cm^{-1}) with a KBr pellet for the documentation of the spectra (ALPHA-Bruker Optics, Germany) was used to investigate the functional group. Thermogravimetry-derivative thermogravimetry TG-DTG, differential thermal analysis (DTA) was performed using Labsys Evo (AF) setaram equipment in airflow under non-isothermal conditions.

The pH point zero charges (pHPZC) are defined by a conventional technique (Hsini *et al.* 2020b) that involves preparing solutions of KNO_3 (60 ml, 0.03 M) and altering their pH to obtain values varying from 2 to 12 by adding HCl or NaOH (0.1 M). Later, the adsorbent (0.45 g) was added to every solution. The mix was kept at room temperature for 24 h under stirring prior to pH_{final} calculation. The curve of pH_{final}-$pH_{initial} = f(pH_{initial})$ was computed to obtain the pH_{PZC}.

2.3. Adsorbate

The commercial-grade Crystal violet (CV) ($C_{25}H_{30}N_3Cl$, M = 408 g/mol and λ_{max} = 584 nm) was acquired from Sigma-Aldrich, and no additional purification was applied. The structure of the CV is displayed in Figure 1. An initial solution of 1,000 mg/L was obtained by adding CV powder (1 g) into distilled water (350 mL) followed by a dilution of 1,000 mL. The dilution of the initial solution into the needed concentrations was done using distilled water.

2.4. Batch experimental

The adsorption measurements were performed in 250 ml conical flasks by pouring 60 ml of CV aqueous solutions with specified concentrations into a defined amount of the adsorbent. The mix was stirred at 120 rpm and at a steady temperature (30 °C) for 240 min. At a fixed time, the stirring was stopped, and the samples were filtered by centrifugal separation. The remaining concentration of the dye in the reaction mix was evaluated via UV2300 spectrophotometer. Adsorption tests were performed by changing pH of the initial solution, time of contact, amount of the adsorbent, concentration initial of CV, and temperature for kinetics of adsorption, isotherms of adsorption, and thermodynamic study. The experiments were performed in triplicates, and the average values were used for experimental data evaluation.

The adsorption percentage R (%) and the adsorption capacity Qe (mg/g) were determined by the equations below (Hsini *et al*. 2021c; Imgharn *et al.* 2021):

$$R(\%) = \frac{(C_0 - C_e)}{C_0} \times 100 \quad (1)$$

$$Q_e = \frac{(C_0 - C_e)}{m} \times V \quad (2)$$

C_0 is the initial concentration of CV (mg/L), C_t denotes the concentration of CV at time t, V is defined as the volume of solution (L), and m symbolizes the mass of adsorbents in g. The entire findings are, in general, reproducible within $\pm$10%. Experiments at the equilibrium were carried out via the above method with a broad array of initial CV concentrations. The time of contact between solid-liquid was 240 min, which was higher than the equilibrium time.

3. RESULTS AND DISCUSSION

3.1. Arg-heliotrope leaves characterization

3.1.1. Surface morphology

SEM images help to observe the surface morphology of adsorbents at micron levels, and SEM is widely used to observe the arrangement of particles on the surface of adsorbents. In the present study, the SEM image of the raw used heliotrope leaves, arginine modified heliotrope leaves before (Arg@HL) and after CV adsorption (Arg@HL-CV) are represented in Figure 2(a)–2(c), respectively. It is indicated from Figure 2(a), that the surface and pores of heliotrope leaves were rough and not

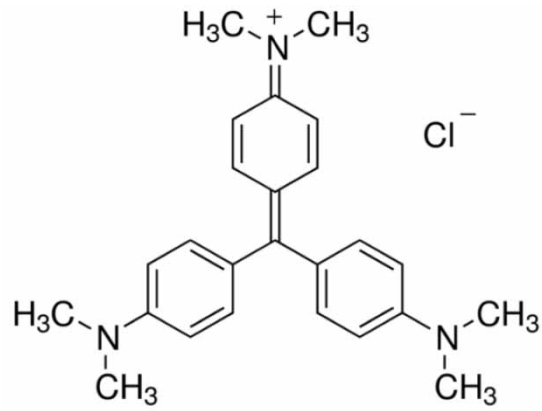

Figure 1 | The structural formula of crystal violet.

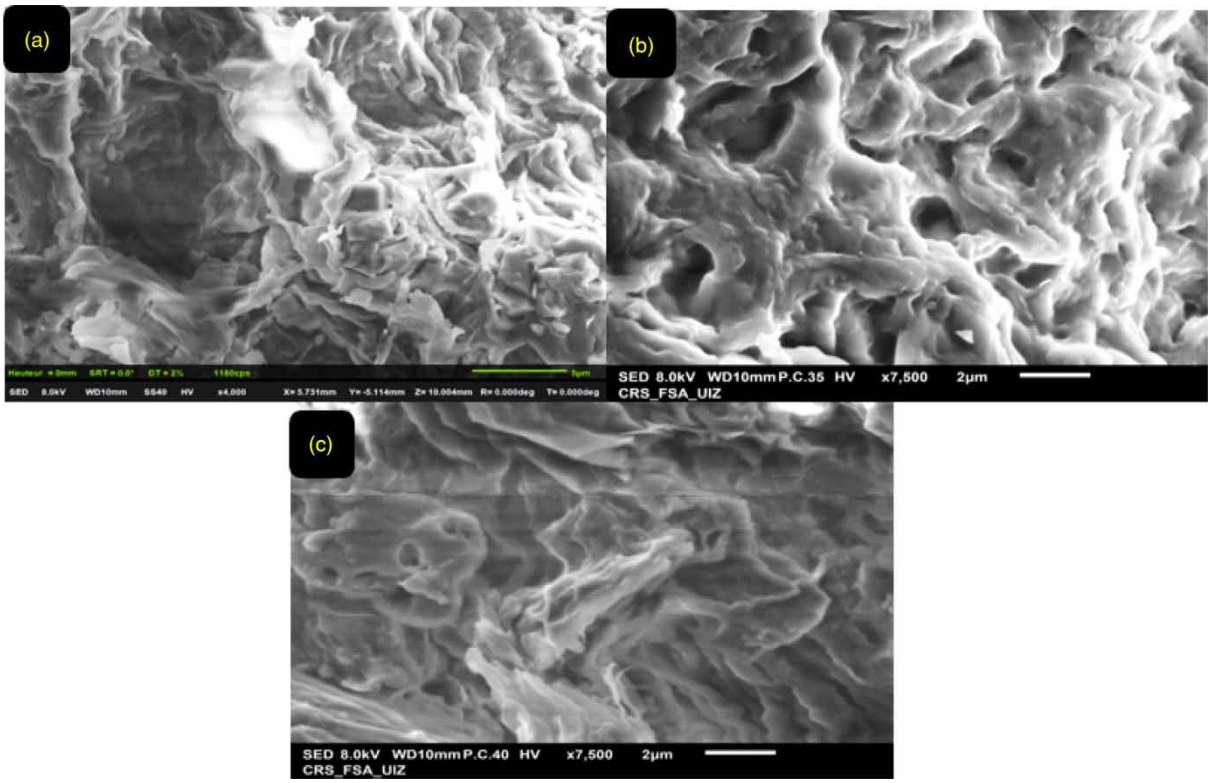

Figure 2 | SEM images of (a) the raw used heliotrope leaves. Arginine-modified heliotrope leaves (Arg@HL) (b) before and (c) after CV adsorption (Arg@HL-CV).

adequately developed. However, in Figure 2(b), several pores with a diameter within the range of 1–6 μm are observed and formed on the arginine-modified heliotrope leaves' surface (Arg@HL). This indicates that the surface coating of the heliotrope leaves by the amino functions arginine leads to the generation of fine pores in the Arg@HL. These pores are expected to enhance the adsorption process as a result of their porosity. This indicates that the arginine has contributed to the widening and formation of pores on the HL surface, which is one of the properties of a good adsorbent that will be efficient in the removal of dyes (Hsini *et al.* 2020a), thus confirming the ability of Arg@HL in removing CV dye under consideration due to the availability of pores of the adsorbent (Ahmad *et al.* 2021). After the adsorption process, the surface of Arg@HL (Figure 2(c)) was covered with CV dye, and the surface of Arg@HL became smooth in a short time. According to the results, we assumed there were physico-chemical adsorption mechanisms on the surface of Arg@HL. As a result of these differences between SEM results, we determined that CV dye was physicochemically adsorbed on the surface of Arg@HL, and this result was supported by UV and FTIR results.

3.1.2. FTIR analysis

FTIR is a vital technique to define the characteristic functional groups that lead to the adsorption performance. The spectrum of Arg-heliotrope leaves before and after the adsorption of CV is exhibited in Figure 3. The FTIR spectrum of Arg@HL indicates several peaks of absorption, implying the intricate nature of the adsorbent. The wide-band at 3,440 cm^{-1} was ascribed to O–H bond vibration stretch overlapped with N-H stretching groups on the surface of Arg@HL surface (Naushad *et al.* 2019b). The weak peak at 2920 cm^{-1} was attributed to the asymmetric C-H stretching present in biomass structure (cellulose, hemicellulose, lignin) (El Messaoudi *et al.* 2016a). The symmetrical stretch vibration of C-H gave rise to the peak at 2,855 cm^{-1} (Han *et al.* 2011; El Messaoudi *et al.* 2016b). The absorption peak at ~1,628 cm^{-1} was the characteristic of stretch vibration of C = O from carboxylic acid with intermolecular hydrogen bond and bending –NH (Han *et al.* 2011; Naushad *et al.* 2019b). The band at 1,530 cm^{-1} was linked to the C = C aromatic stretching of lignin (Han *et al.* 2011). The bands at 1,472 cm^{-1} and 1,347 cm^{-1} were credited to the vibration C–O of methoxy groups of lignin (El Messaoudi *et al.* 2016a). The bands at

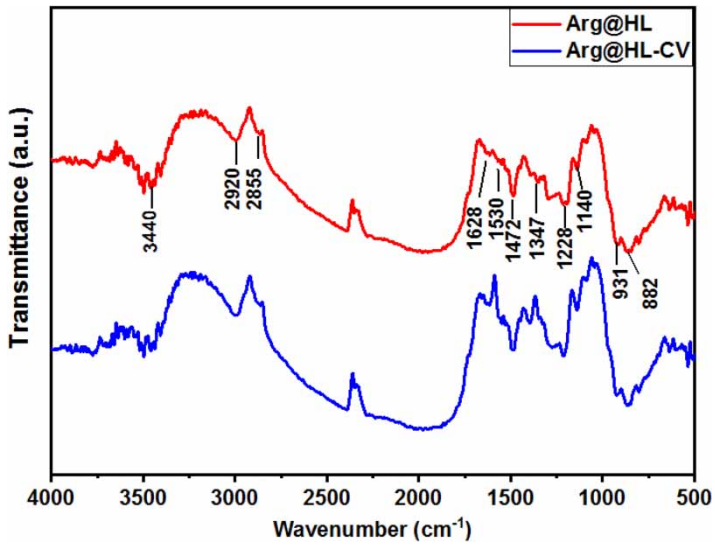

Figure 3 | FTIR spectrums of Arg-heliotrope leaves (Arg@HL) and CV loaded Arg-heliotrope leaves (Arg@HL-CV).

1228 cm^{-1} were C–O stretching vibration of carboxylic acids and alcohols (El Messaoudi *et al.* 2016a, 2016b). The peaks between 1,140 cm^{-1} and 931 cm^{-1} correspond to stretching vibrations of C–O, and C–O–C bonds of cellulose (Peydayesh & Rahbar-Kelishami 2015). The band at 882 cm^{-1} was ascribed to C–H deformation in cellulose (Deniz & Kepekci 2016). After adsorption of CV, we noted that the peaks intensity of O–H, C = O, and C–O were shifted from 3,440 cm^{-1}, 1,628 $cm^{-1,}$ and 1,228 cm^{-1} to 3,450 cm^{-1}, 1,631 $cm^{-1,}$ and 1,033 cm^{-1}, respectively. This indicates that interaction has occurred between CV and these groups. These results showed that the Arg@HL contains several functional groups belonging to the CV such as O–H, C = O, and C–O.

3.1.3. Thermal analysis Arg-heliotrope leaves

Thermo-gravimetric analysis (TGA) is a thermal analysis technique that evaluates the correlation between the sample's mass and temperature change under programmed temperature control. The thermogravimetric and heat flow profiles of Arg-heliotrope leaves prior to and following CV dye adsorption are displayed in Figure 4. The analysis was conducted at a temperature range of 33 °C–900 °C. The TGA curve of the Arg-heliotrope leaves composite demonstrates a standard four-stage weight-loss performance. The initial thermal degradation phase reveals a 5% weight-loss obtained under 100 °C, which was assigned to the physisorbed water desorption. In the second stage, the TGA curve demonstrated a 9.82% weight loss up to 250 °C, attributed to the organic matter's pyrolysis, as well as the release of some light gases such as CO_2 and CO and volatile elements;

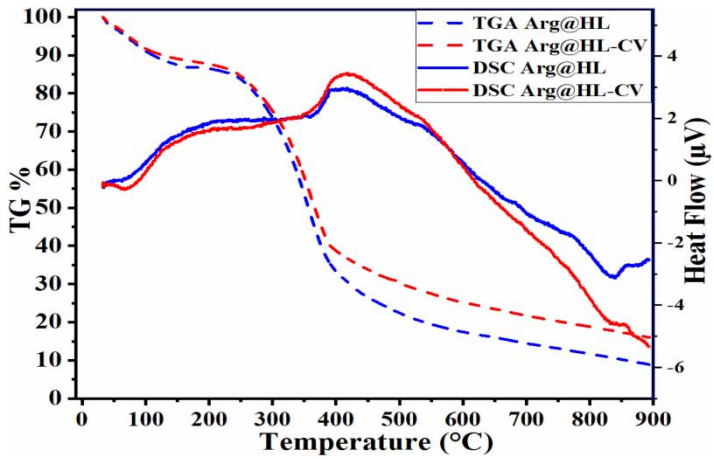

Figure 4 | DSC/TGA thermograms of Arg-heliotrope leaves prior and following adsorption of CV dye.

identical results were reported by Mahmood *et al.* (2017). The third stage displayed a continuing weight loss of 59% at 450 °C, which could be because of the cellulose thermal decay, hemicelluloses, and lignin as described by Yagmur *et al.* (2008). Additionally, this behavior is also apparent in the DTA exothermic peaks noted in this temperature range. The 17.6% defined as the last weight loss was determined in the 450 °C–900 °C temperature range, which might be attributed to the lignin degradation (Mahmood *et al.* 2017).

A comparative study of DTA curves of Arg-heliotrope leaves prior and following CV dye's adsorption does not show any major deviation in the thermal stability. Furthermore, compared with the 8.67 wt% residual left for the Arg@HL at 900 °C, 15.69 wt% residue weight was discovered for the Arg@HL-CV composite. This outcome additionally verified CV dye's adsorption on the Arg- heliotrope leaves surface (Hsini *et al.* 2021a).

3.2. Adsorption analysis

3.2.1. Influence of adsorbent dosage

The dosage of adsorbent is a valuable chemical factor since it establishes the adsorbent's capacity for a provided quantity of the adsorbent at the working conditions. Figure 5 demonstrates that the proportion of dye elimination at equilibrium was enhanced from 50.16 to 99.39% with the adsorbent mass increase from 0.125 to 3 $g{\cdot}L^{-1}$. Nevertheless, the adsorption capacity revealed a declining tendency with rising adsorbent quantity. If the adsorbent amount is enhanced by maintaining the CV concentration constant, the amount of CV adsorbed per unit mass declined due to fewer CV ions being present in the mass of the adsorbent. The capacity of adsorption declined from 80.26 to 6.62 mg/g with an increase of adsorbent quantity (from 0.125 to 0.3 g/L). The reduction in adsorption capacity is primarily assigned to the unsaturation of the sites during the adsorption procedure. For the 0.75 g/L of adsorbent quantity, the optimum values of CV elimination and adsorption capacity are discovered to be 96.54% and 25.74 mg/g, respectively.

3.2.2. Effect of initial pH

The pH is a significant parameter since it influences the adsorbent's protonation and deprotonation as well as the adsorbate's functional groups, taming their electrostatic interaction (Hsini *et al.* 2020a). In this regard, the cationic dye CV's adsorption is influenced by the solution's pH because of the highly pH-dependent mechanisms, like ion exchange, complexation, or electrostatic retention forces (Kosmulski 2016). For this reason, the pH influence on the CV adsorption towards pure Leaves (HL) or modified Arg-Leaves surface sites (Arg@HL) was considered in a pH range of 2–12, the solutions were regulated to the chosen values by the addition of HCl (0.1 N) and NaOH (0.1 N), while the concentration of the CV was kept at 20 mg/L, the temperature at 298 K and the mass of the pristine Leaves or modified Arg-Leaves adsorbent at 0.75 $g{\cdot}L^{-1}$. It was noticed that CV adsorption on the Leaves and modified Arg-Leaves surface is extremely pH-dependent. In an acidic medium, at pH below 6, the adsorption percent increased by improving the initial pH. Optimal CV adsorption was reached at pH >6.

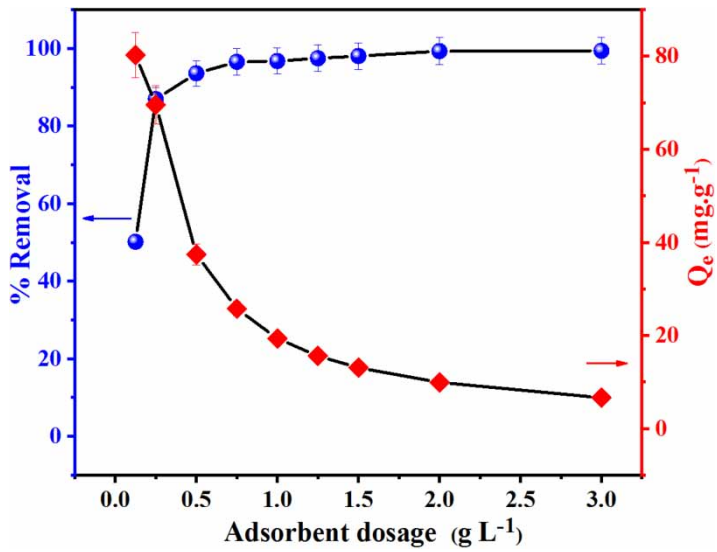

Figure 5 | CV dye adsorption as a function of Arg@HL dose ($C_0 = 20$ $mg{\cdot}L^{-1}$, adsorption time = 240 min, T = 298 K and pH = 6).

Moreover, Leaves' PZC values and that of modified Arg- Leaves were observed to be 6.5 and 7.0 (inset in Figure 6), respectively. At pH < PZC, the CV molecules and the surfaces of adsorbents have the same charges. This triggers adsorbate-adsorbent repulsive interactions and consequently inhibits the CV adsorption. Additionally, the CV elimination efficacy diminished with reducing pH of the solution due to the increase of repulsions phenomenon. Hence, strong competition between CV and H^+ ions towards adsorbent active sites can not be overlooked in acidic environments. Furthermore, CV adsorption for pristine Leaves and modified Arg-Leaves surface sites at pH > PZC, was mainly supported by the phenomenon of electrostatic attraction occurring between cationic CV dye and negatively charged adsorbent surface sites (deprotonated functional groups).

3.2.3. Adsorption equilibrium and thermodynamic study

The equilibrium of adsorption isotherms carries a crucial part in examining CV dye molecules' distribution at the liquid/Arg-leaves interface. The investigation of the adsorption at the equilibrium was conducted in the optimal experimental factors. Langmuir (Langmuir 1917) and Freundlich (Ba Mohammed *et al.* 2020) isothermal models were employed to describe the CV dye adsorption equilibrium on the Arg-leaves surface. The Langmuir isotherm theory adopts a monolayer adsorbate coverage over a homogeneous adsorbent surface where each site of adsorption is the same and energetically equal (Langmuir 1917). In contrast, the Freundlich isotherm model is appropriate for a heterogeneous adsorbent surface with multilayer adsorption and expects that the adsorbate concentration on the adsorbent will improve when absorbate concentration in the solution increases (Ba Mohammed *et al.* 2020). The CV adsorption over the Arg-leaves surface along with the fitted Langmuir and Freundlich isotherms are presented in Figure 7(a). The values of the parameter are displayed in Table 1. The regression coefficient values comparison revealed that the Langmuir model is more fitted to explain CV adsorption over the Arg@HL than Freundlich. Though the computed Langmuir monolayer uptake capacity ($Q_m = 475.5\ mg{\cdot}g^{-1}$) was reasonably adapted to the practical value ($Q_{m.exp} = 401.2\ mg{\cdot}g^{-1}$). Consequently, the adsorption of CV onto the Arg@HL is a monolayer coverage on the binding sites that are energetically homogeneous, as described by the Langmuir model.

The highest adsorption capacity of Arg@HL for CV was matched with the results of several adsorbents defined in the literature, as depicted in Table 2.

From Table 2, it could be assumed that Arg@HL shows a high or equivalent capacity of adsorption compared to other low-cost adsorbent materials. This higher adsorption capacity for CV removal by Arg@HL compared to other adsorbents was due to the functionalization by arginine, which means gaining more functions, which favors the interactions between the functions of the adsorbent and the CV dye molecules.

To explain the thermodynamic conduct of the adsorption procedure, the thermodynamic factors like free enthalpy ($\Delta G°$), enthalpy ($\Delta H°$), and entropy ($\Delta S°$) were acquired from the study of the temperature effect on the adsorption of CV onto

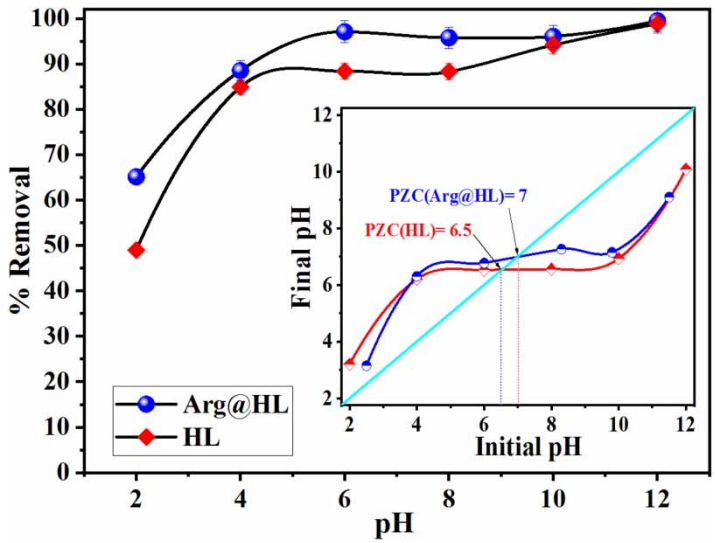

Figure 6 | pH influence on the efficiency of CV dye adsorption in the presence of HL and Arg@HL ($C_0 = 20\ mg{\cdot}L^{-1}$, time of adsorption = 240 min, adsorbent amount = 0.75 g/L and T = 298 K). The inset is the PZC of HL and Arg@HL.

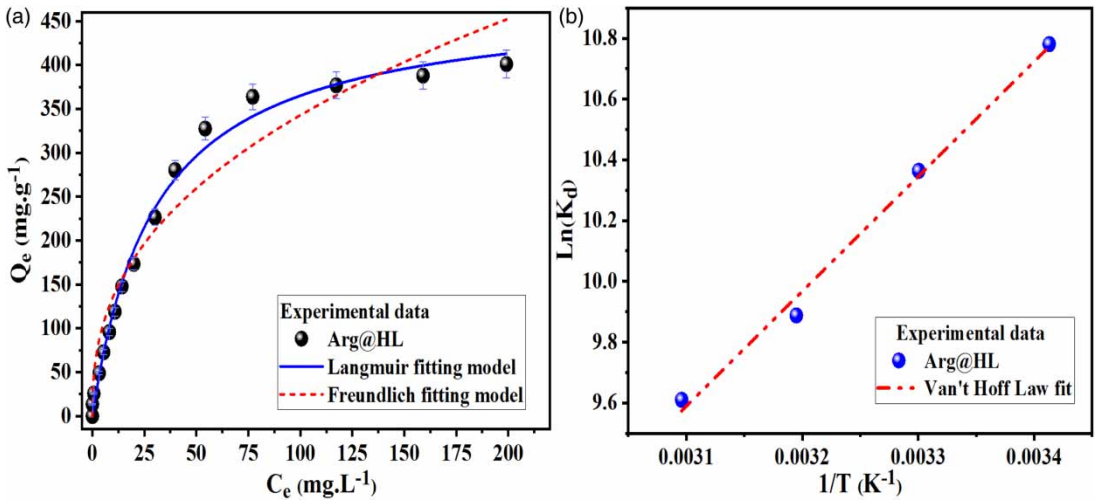

Figure 7 | (a) Non-linear Langmuir and Freundlich isotherm plots for the adsorption of CV on the Arg@HL and **(b)** plot determining thermodynamic factors.

Table 1 | Nonlinear regression parameters of Langmuir and Freundlich models for CV adsorption on the Arg@HL

		Langmuir $Q_e = \frac{Q_{max} K_L C_e}{1 + K_L C_e}$			Freundlich $Q_e = K_F C_e^{1/n}$		
Adsorbent	Q_{exp} (mg.g^{-1})	Q_{max} (mg.g^{-1})	K_L (L.mg^{-1})	R^2	n_f	K_F (mg.g^{-1})	R^2
Arg@HL	401.2	475.5	0.0331	0.9931	2.492	54.04	0.9486

Arg@HL. Evaluation of the results was conducted using Equations (3) and (4) (Hsini *et al.* 2020a, 2020b).

$$LnK_d = \frac{\Delta S^\circ}{R} - \frac{\Delta H^\circ}{RT} \tag{3}$$

K_d: constant distribution equilibrium specified by the subsequent equation:

$$K_d = \frac{Q_d}{C_e} \tag{4}$$

where T (K) is absolute temperature, R = 8.314 J mol^{-1} K^{-1}, and ρ (mg/l) means water density.

Table 2 | Comparison of the maximum uptake capacities of Arg@HL for CV removal and other adsorbents addressed in the previously published studies

Material	Q_{max} (mg.g^{-1})	Reference
H_2SO_4 treated *Cucumis sativus*	12.09	Smitha *et al.* (2017)
Acid activated sintering process red mud	21	Zhang *et al.* (2014)
Alginate/acid activated bentonite	390.7	Oladipo & Gazi (2014)
EDTA-Cross-Linked β-cyclodextrin	104.03	Yao *et al.* (2015)
Glutamic acid modified chitosan magnetic composite	371.5	Yan *et al.* (2013)
Chitosan magnetic composite	86.6	Yan *et al.* (2013)
Arg@HL	**475.5**	Current study

The thermodynamic factors (ΔG°, ΔH°, and ΔS°) obtained from ln Kd Vs. 1/T plot (Figure 7(b)) are represented in Table 3. ΔG° evaluated at all temperatures was negative, which means that the adsorption process is spontaneous (Hsini *et al.* 2020a, 2020b). The adsorption of CV onto Arg@HL is an endothermic reaction proven by the obtained negative $\Delta H°$ values. ΔS° is used to define the ion exchange at the interface of the solid-liquid through the adsorption process. The obtained ΔS° was also negative, endorsing the exothermic nature of the adsorption of CV onto Arg@HL (Sharma *et al.* 2018; Naushad *et al.* 2019b).

3.2.4. Adsorption kinetics

The kinetics data corresponding to the CV adsorption on Arg@HL was additionally mimicked via three frequently employed models: pseudo-first-order Langmuir, pseudo-second-order Ho, and Weber-Morris intraparticle diffusion models. For the pseudo-first-order model, as noticed in Figure 8(a), k_1 and q_e values are defined from the log (q_e-q_t) vs. t plot. k_2 and q_e values for the pseudo-second-order model were concluded from the t/q_t versus t plot. The intraparticle model constants were established from the intercept and qt's plot's slope vs. t (Figure 8(b)). The kinetic data were evaluated by the kinetic equation stated above, and assessed parameters were presented in Table 4. The correlation coefficient (R^2) found using pseudo-second-order kinetics (0.9803) were superior to those from the kinetics of the pseudo-first-order (0.9342). The $q_{e,2cal}$ were closer to ($q_{e,exp}$) obtained experimentally, proving pseudo-second-order suitability for predicting the data experimentally. An excellent ionic interplay strength between the Arg@HL and CV (Ba Mohammed *et al.* 2020) was revealed via the model of pseudo-second-order, which agrees with the pH and the amount of adsorbent effect.

CONCLUSION

In the present work, Heliotrope leaf modified by arginine (Arg@HL) was synthesized and applied as an adsorbent for the removal of CV dye from an aqueous medium. The adsorbent was characterized using different instrumental techniques viz., SEM, FTIR, TGA and DSC. Batch method experiments were carried out at room temperature to study the influence

Table 3 | The values of thermodynamic parameters related to CV dye adsorption onto Arg@HL

			ΔG°(kJ.mol^{-1})			
Adsorbent	**ΔH° (kJ.mol^{-1})**	**ΔS° (J.mol^{-1}.K^{-1})**	**293 K**	**303 K**	**313 K**	**323 K**
Arg@HL	−31.42	−17.71	−26.25	−26.09	−25.72	−25.80

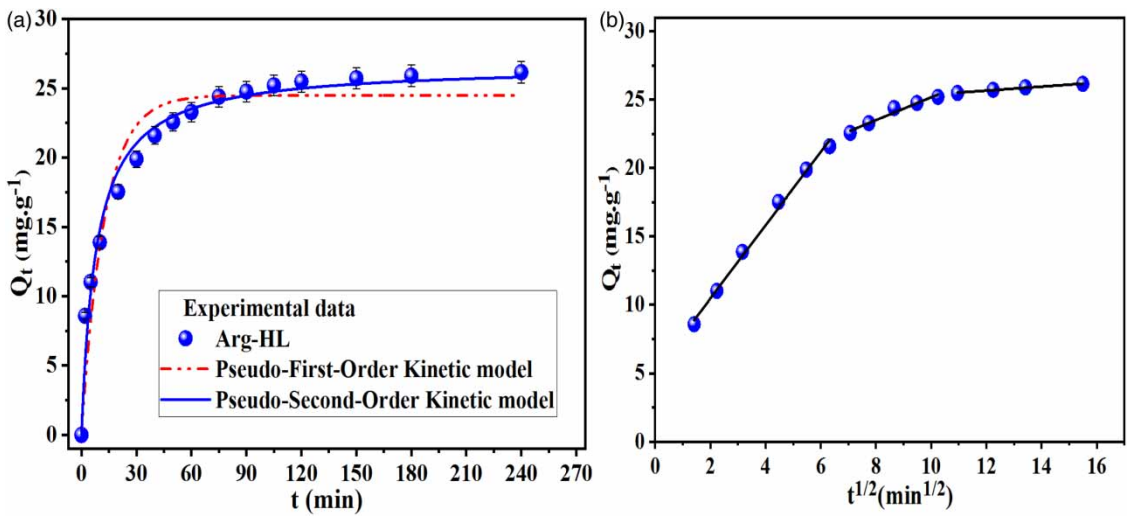

Figure 8 | Pseudo-first order, pseudo-second-order (a), and Weber-Morris intraparticle diffusion linear (b) plots for CV dye adsorption by Arg@HL.

Table 4 | Parameters of PFO, PSO, and IPD models for CV adsorption onto Arg@HL composite from aqueous medium

		PFO model $Q_t = Q_e(1 - \exp(-k_{PSO}t))$			PSO model $Q_t = \frac{Q_e^2 k_{PSO} t}{1 + Q_e k_{PSO} t}$		
Adsorbent	$Q_{e.exp}$ (mg.g^{-1})	k_1	$Q_{e.1}$	R^2	k_2	$Q_{e.2}$	R^2
Arg@HL	26.15	0.081	24.48	0.9342	4.66×10^{-4}	26.66	0.9803

	IPD model $Q_t = k_{IPD}t^{1/2} + \beta$								
	Initial linear portion			**Second linear portion**			**Third linear portion**		
	$k_{IPD.1}$	β_1	R^2	$k_{IPD.2}$	β_2	R^2	$k_{IPD.3}$	β_3	R^2
Arg@HL	2.68	5.11	0.9953	0.83	16.84	0.9650	0.15	23.92	0.9886

Note: k_{PFO}(min^{-1}), k_{PSO}(mg.g^{-1}.min^{-1}) and k_{IPD}(mg.g^{-1}.min$^{-0.5}$) designate the PFO, PSO and IPD rate constants, respectively. β(mg.g^{-1}) indicates the boundary layer thickness. Q_e and Q_t stand for amounts (mg·g^{-1}) of CV adsorbed at equilibrium and time t, respectively.

of different parameters on adsorption of CV onto Arg@HL. The results showed that the amount of CV dye adsorption was found to increase with the increase in initial dye concentration, contact time, amount of adsorbent, system temperature, and solution pH. It was found that the optimum capacity of adsorption of CV on Arg@HL is in the order of 25.74 mg·g^{-1} with a removal percentage of 96.54% for a CV concentration of 20 mg·L^{-1}, an amount of 0.75 g·L^{-1} of the adsorbent, pH = 6, and a temperature of 298 K. Moreover, Langmuir and pseudo-second order models were the most satisfying models to describe the adsorption phenomenon. The obtained results lead to the conclusion that the Arg@HL adsorbent is considered as highly efficient and eco-friendly material for textile dyes removal from industrial waste effluents.

DATA AVAILABILITY STATEMENT

All relevant data are included in the paper or its Supplementary Information.

REFERENCES

Aarab, N., Hsini, A., Essekri, A., Laabd, M., Lakhmiri, R. & Albourine, A. 2020a Removal of an emerging pharmaceutical pollutant (metronidazole) using PPY-PANi copolymer: kinetics, equilibrium and DFT identification of adsorption mechanism. *Groundwater Sustainable Dev.* **11**, 100416. https://doi.org/10.1016/j.gsd.2020.100416.

Aarab, N., Hsini, A., Laabd, M., Essekri, A., Laktif, T., Haki, M. A., Lakhmiri, R. & Albourine, A. 2020b Theoretical study of the adsorption of sodium salicylate and metronidazole on the PANi. *Mater. Today Proc.* **22**, 100–103. https://doi.org/10.1016/j.matpr.2019.08.103.

Abdellaoui, Y., Abou Oualid, H., Hsini, A., El Ibrahimi, B., Laabd, M., El Ouardi, M., Giácoman-Vallejos, G. & Gamero-Melo, P. 2021 Synthesis of zirconium-modified Merlinoite from fly ash for enhanced removal of phosphate in aqueous medium: experimental studies supported by Monte Carlo/SA simulations. *Chem. Eng. J.* **404**, 126600. https://doi.org/10.1016/j.cej.2020.126600.

Ahmad, M. A., Ahmed, N. B., Adegoke, K. A. & Bello, O. S. 2021 Adsorptive potentials of lemongrass leaf for methylene blue dye removal. *Chem. Data Collect.* **31**, 100578. https://doi.org/10.1016/j.cdc.2020.100578.

Ait Ahsaine, H., Slassi, A., Naciri, Y., Chennah, A., Jaramillo-Páez, C., Anfar, Z., Zbair, M., Benlhachemi, A. & Navío, J. A. 2018 Photo/Electrocatalytic properties of nanocrystalline ZnO and La–Doped ZnO: combined DFT fundamental semiconducting properties and experimental study. *ChemistrySelect.* **3**, 7778–7791. https://doi.org/10.1002/slct.201801729.

Ajmal, Z., Muhmood, A., Usman, M., Kizito, S., Lu, J., Dong, R. & Wu, S. 2018 Phosphate removal from aqueous solution using iron oxides: adsorption, desorption and regeneration characteristics. *J. Colloid Interface Sci.* **528**, 145–155. https://doi.org/10.1016/j.jcis.2018.05.084.

Ajmal, Z., Muhmood, A., Dong, R. & Wu, S. 2020a Probing the efficiency of magnetically modified biomass-derived biochar for effective phosphate removal. *J. Environ. Manage.* **253**, 109730. https://doi.org/10.1016/j.jenvman.2019.109730.

Ajmal, Z., Usman, M., Anastopoulos, I., Qadeer, A., Zhu, R., Wakeel, A. & Dong, R. 2020b Use of nano-/micro-magnetite for abatement of cadmium and lead contamination. *J. Environ. Manage.* **264**, 110477. https://doi.org/10.1016/j.jenvman.2020.110477.

Ajmal, Z., Naciri, Y., Hsini, A., Bresolin, B. M., Qadeer, A., Muhammad Nauman, M. A., Muhammad Kashif Irshad, K. A. K., Djellabi, R., Bianchi, C. L., Laabd, M., Albourine, A. & Dong, R. 2021 *Prospects of Photocatalysis in the Management of Nitrate Contamination in Potable Water*.

Akhsassi, B., Bouddouch, A., Naciri, Y., Bakiz, B., Taoufyq, C. F. A., Villain, S., Guinneton, F. & Benlhachemi, A. 2021 Enhanced photocatalytic activity of $Zn_3(PO_4)_2$/ZnO composite semiconductor prepared by different methods. *Chem. Phys. Lett.* **783**, 139046.

Ba Mohammed, B., Hsini, A., Abdellaoui, Y., Abou Oualid, H., Laabd, M., El Ouardi, M., Ait Addi, A., Yamni, K. & Tijani, N. 2020 Fe-ZSM-5 zeolite for efficient removal of basic Fuchsin dye from aqueous solutions: synthesis, characterization and adsorption process optimization using BBD-RSM modeling. *J. Environ. Chem. Eng.* **8**, 104419. https://doi.org/10.1016/j.jece.2020.104419.

Barebita, H., Naciri, Y., Ferraa, S., Nimour, A. & Guedira, T. 2020 Investigation of structural and photocatalytic behavior of $Bi_{13}B_{1-2x}V_xP_xO_{20.95+2x}$ $(0 \leq x \leq 0.5)$. *Solid State Sci.* **108**, 106389. https://doi.org/10.1016/j.solidstatesciences.2020.106389.

Benafqir, M., Hsini, A., Laabd, M., Laktif, T., Ait Addi, A., Albourine, A. & El Alem, N. 2019 Application of density functional theory computation (DFT) and process capability study for performance evaluation of orthophosphate removal process using Polyaniline@ Hematite-titaniferous sand composite (PANI@HTS) as a substrate. *Sep. Purif. Technol.* **236**, 116286. https://doi.org/10.1016/j.seppur.2019.116286.

Bouziani, A., Park, J. & Ozturk, A. 2020 Synthesis of α-Fe_2O_3/TiO_2 heterogeneous composites by the sol-gel process and their photocatalytic activity. *J. Photochem. Photobiol. A Chem.* **400**, 112718. https://doi.org/10.1016/j.jphotochem.2020.112718.

Bouziani, A., Park, J. & Ozturk, A. 2021 Effects of fluorination and thermal shock on the photocatalytic activity of Bi_2O_3 nanopowders. *Colloids Surf., A* **626**, 127049. https://doi.org/10.1016/j.colsurfa.2021.127049.

Chennah, A., Naciri, Y., Ahsaine, H. A., Taoufyq, A., Bakiz, B., Bazzi, L., Guinneton, F., Gavarri, J.-R. & Benlhachemi, A. 2018 Electrocatalytic properties of hydroxyapatite thin films electrodeposited on stainless steel substrates, Mediterr. *J. Chem.* **6**. https://doi.org/10.13171/mjc66/01712241118-gavarri.

Chennah, A., Naciri, Y., Taoufyq, A., Bakiz, B., Bazzi, L., Guinneton, F., Villain, S., Gavarri, J. R. & Benlhachemi, A. 2019 Electrodeposited zinc phosphate hydrate electrodes for electrocatalytic applications. *J. Appl. Electrochem.* **49**, 163–177. https://doi.org/10.1007/s10800-018-1261-8.

Deniz, F. & Kepekci, R. A. 2016 Dye biosorption onto pistachio by-product: a Green environmental engineering approach. *J. Mol. Liq.* **219**, 194–200. https://doi.org/10.1016/j.molliq.2016.03.018.

El messaoudi, N., Elkhomri, M., Dbik, A., Bentahar, S., Lacherai, A. & Bakiz, B. 2016a Biosorption of Congo red in a fixed-bed column from aqueous solution using jujube shell: experimental and mathematical modeling. *J. Environ. Chem. Eng.* **4**, 3848–3855. https://doi.org/10.1016/j.jece.2016.08.027.

El Messaoudi, N., El Khomri, M., Bentahar, S., Dbik, A., Lacherai, A. & Bakiz, B. 2016b Evaluation of performance of chemically treated date stones: application for the removal of cationic dyes from aqueous solutions. *J. Taiwan Inst. Chem. Eng.* **67**, 244–253. https://doi.org/10.1016/j.jtice.2016.07.024.

Erdogan, N., Bouziani, A., Park, J., Micusik, M., Kim, S. Y., Majkova, E., Omastova, M. & Ozturk, A. 2019 Synthesis and enhanced photocatalytic activity of nitrogen-doped triphasic TiO_2 nanoparticles. *J. Photochem. Photobiol. A Chem.* **377**, 92–100. https://doi.org/10.1016/j.jphotochem.2019.03.047.

Essekri, A., Hsini, A., Naciri, Y., Laabd, M., Ajmal, Z., El Ouardi, M., Ait Addi, A. & Albourine, A. 2020 Novel citric acid-functionalized brown algae with a high removal efficiency of crystal violet dye from colored wastewaters: insights into equilibrium, adsorption mechanism, and reusability. *Int. J. Phytoremediation.* **23**, 1–11. https://doi.org/10.1080/15226514.2020.1813686.

Fegousse, A., El Gaidoumi, A., Miyah, Y., El Mountassir, R. & Lahrichi, A. 2019 Pineapple bark performance in dyes adsorption: optimization by the central composite design. *J. Chem.* **2019**. https://doi.org/10.1155/2019/3017163.

Ferraa, S., Naciri, Y., Hsini, A., Barebita, H., Bouziani, A., Albourine, A., Nimour, A. & Guedira, T. 2020 Evolution of the physicochemical and photocatalytic properties of BaO embedded in bismuth phosphovanadates glasses. *Chem. Phys. Lett* 138173. https://doi.org/10.1016/j.cplett.2020.138173.

Garg, V. K., Kumar, R. & Gupta, R. 2004 Removal of malachite Green dye from aqueous solution by adsorption using agro-industry waste: a case study of *Prosopis cineraria*. *Dye. Pigment.* **62**, 1–10. https://doi.org/10.1016/j.dyepig.2003.10.016.

Gharbani, P., Tabatabaii, S. M. & Mehrizad, A. 2008 Removal of Congo red from textile wastewater by ozonation. *Int. J. Environ. Sci. Technol.* **5**, 495–500. https://doi.org/10.1007/BF03326046.

Han, X., Wang, W. & Ma, X. 2011 Adsorption characteristics of methylene blue onto low cost biomass material lotus leaf. *Chem. Eng. J.* **171**, 1–8. https://doi.org/10.1016/j.cej.2011.02.067.

Hasanzadeh, M., Simchi, A. & Shahriyari Far, H. 2020 Nanoporous composites of activated carbon-metal organic frameworks for organic dye adsorption: synthesis, adsorption mechanism and kinetics studies. *J. Ind. Eng. Chem.* **81**, 405–414. https://doi.org/10.1016/j.jiec.2019.09.031.

Hsini, A., Naciri, Y., Laabd, M., El Ouardi, M., Ajmal, Z., Lakhmiri, R., Boukherroub, R. & Albourine, A. 2020a Synthesis and characterization of arginine-doped polyaniline/walnut shell hybrid composite with superior clean-up ability for chromium (VI) from aqueous media: equilibrium, reusability and process optimization. *J. Mol. Liq.* **316**, 113832. https://doi.org/10.1016/j.molliq.2020.113832.

Hsini, A., Essekri, A., Aarab, N., Laabd, M., Addi, A. A., Lakhmiri, R. & Albourine, A. 2020b Elaboration of novel polyaniline@Almond shell biocomposite for effective removal of hexavalent chromium ions and Orange G dye from aqueous solutions. *Environ. Sci. Pollut. Res.* **27**, 1–14. https://doi.org/10.1007/s11356-020-08039-1.

Hsini, A., Naciri, Y., Benafqir, M., Ajmal, Z., Aarab, N., Laabd, M., Navío, J. A., Puga, F., Boukherroub, R., Bakiz, B. & Albourine, A. 2021a Facile synthesis and characterization of a novel 1,2,4,5-benzene tetracarboxylic acid doped polyaniline@zinc phosphate nanocomposite for highly efficient removal of hazardous hexavalent chromium ions from water. *J. Colloid Interface Sci.* **585**, 560–573. https://doi.org/10.1016/j.jcis.2020.10.036.

Hsini, A., Naciri, Y., Laabd, M., Bouziani, A., Navío, J., Puga, F., Boukherroub, R., Lakhmiri, R. & Albourine, A. 2021b Development of a novel PANI@WO3 hybrid composite and its application as a promising adsorbent for Cr(VI) ions remova. *J. Environ. Chem. Eng.* **9**, 105885.

Hsini, A., Benafqir, M., Naciri, Y., Laabd, M., Bouziani, A., Ez-zahery, M., Lakhmiri, R., El Alem, N. & Albourine, A. 2021c Synthesis of an arginine-functionalized polyaniline@FeOOH composite with high removal performance of hexavalent chromium ions from water: adsorption behavior, regeneration and process capability studies. *Colloids Surfaces A Physicochem. Eng. Asp.* **617**, 126274. https://doi.org/10.1016/j.colsurfa.2021.126274.

Imgharn, A., ighnih, H., Hsini, A., Naciri, Y., Laabd, M., Kabli, H., Elamine, M., Lakhmiri, R., Souhail, B. & Albourine, A. 2021 Synthesis and characterization of polyaniline-based biocomposites and their application for effective removal of Orange G dye using adsorption in dynamic regime. *Chem. Phys. Lett.* **778**, 138811. https://doi.org/10.1016/j.cplett.2021.138811.

Kizito, S., Luo, H., Wu, S., Ajmal, Z., Lv, T. & Dong, R. 2017a Phosphate recovery from liquid fraction of anaerobic digestate using four slow pyrolyzed biochars: dynamics of adsorption, desorption and regeneration. *J. Environ. Manage.* **201**, 260–267. https://doi.org/10.1016/j.jenvman.2017.06.057.

Kizito, S., Lv, T., Wu, S., Ajmal, Z., Luo, H. & Dong, R. 2017b Treatment of anaerobic digested effluent in biochar-packed vertical flow constructed wetland columns: role of media and tidal operation. *Sci. Total Environ.* **592**, 197–205. https://doi.org/10.1016/j.scitotenv.2017.03.125.

Kosmulski, M. 2016 Isoelectric points and points of zero charge of metal (hydr)oxides: 50 years after parks' review. *Adv. Colloid Interface Sci.* **238**, 1–61. https://doi.org/10.1016/j.cis.2016.10.005.

Laabd, M., Imgharn, A., Hsini, A., Naciri, Y., Mobarak, M., Szunerits, S., Boukherroub, R. & Albourine, A. 2022 Efficient detoxification of Cr(VI)-containing effluents by sequential adsorption and reduction using a novel cysteine-doped PANi@faujasite composite: experimental study supported by advanced statistical physics prediction. *J. Hazard. Mater.* **422**, 126857.

Langmuir, I. 1917 The constitution and fundamental properties of solids and liquids. Part II.-Liquids. *J. Franklin Inst.* **184**, 721. https://doi.org/10.1016/s0016-0032(17)90088-2.

Mahmood, T., Ali, R., Naeem, A., Hamayun, M. & Aslam, M. 2017 Potential of used *Camellia sinensis* leaves as precursor for activated carbon preparation by chemical activation with H_3PO_4; optimization using response surface methodology. *Process Saf. Environ. Prot.* **109**, 548–563. https://doi.org/10.1016/j.psep.2017.04.024.

Mimouni, I., Bouziani, A., El Azzouzi, M., Naciri, Y., Boujnah, M. & El Belghiti, M. A. 2021 Effect of heat treatment on the photocatalytic activity of α-Fe_2O_3 nanoparticles: towards diclofenac elimination. *Environ. Sci. Pollut. Res.*, 1–13.

Mittal, A., Mittal, J., Malviya, A., Kaur, D. & Gupta, V. K. 2010 Adsorption of hazardous dye crystal violet from wastewater by waste materials. *J. Colloid Interface Sci.* **343**, 463–473. https://doi.org/10.1016/j.jcis.2009.11.060.

Naciri, Y., Ait Ahsaine, H., Chennah, A., Amedlous, A., Taoufyq, A., Bakiz, B., Ezahri, M., Villain, S. & Benlhachemi, A. 2018 Facile synthesis, characterization and photocatalytic performance of $Zn_3(PO_4)_2$ platelets toward photodegradation of Rhodamine B dye. *J. Environ. Chem. Eng.* **6**, 1840–1847. https://doi.org/10.1016/j.jece.2018.02.009.

Naciri, Y., Chennah, A., Jaramillo-Páez, C., Navío, J. A., Bakiz, B., Taoufyq, A., Ezahri, M., Villain, S., Guinneton, F. & Benlhachemi, A. 2019a Preparation, characterization and photocatalytic degradation of Rhodamine B dye over a novel $Zn_3(PO_4)_2$ /$BiPO_4$ catalyst. *J. Environ. Chem. Eng.* **7**, 103075. https://doi.org/10.1016/j.jece.2019.103075.

Naciri, Y., Bouddouch, A., Bakiz, B., Taoufyq, A., Ezahri, M. & Benlhachemi, A. 2019b Photocatalytic degradation of sulfadiazine by $Zn_3(PO_4)_2$/$BiPO_4$ composites upon UV light irradiation. *Mater. Today Proc.* **3**, 8–11. https://doi.org/10.1016/j.matpr.2019.08.071.

Naciri, Y., Hsini, A., Ajmal, Z., Bouddouch, A., Bakiz, B., Navío, J. A., Albourine, A., Valmalette, J. C., Ezahri, M. & Benlhachemi, A. 2020a Influence of Sr-doping on structural, optical and photocatalytic properties of synthesized $Ca_3(PO_4)_2$. *J. Colloid Interface Sci.* **572**, 269–280. https://doi.org/10.1016/j.jcis.2020.03.105.

Naciri, Y., Hsini, A., Ajmal, Z., Navío, J. A., Bakiz, B., Albourine, A., Ezahri, M. & Benlhachemi, A. 2020b Recent progress on the enhancement of photocatalytic properties of $BiPO_4$ using π–conjugated materials. *Adv. Colloid Interface Sci.* **280**, 102160. https://doi.org/10.1016/j.cis.2020.102160.

Naciri, Y., Hsini, A., Bouziani, A., Djellabi, R., Ajmal, Z., Laabd, M., Navío, J. A., Mills, A., Bianchi, C. L., Li, H., Bakiz, B. & Albourine, A. 2021 Photocatalytic oxidation of pollutants in gas-phase via Ag_3PO_4-based semiconductor photocatalysts: recent progress, new trends, and future perspectives. *Crit. Rev. Environ. Sci. Technol.*, 1–44. https://doi.org/10.1080/10643389.2021.1877977.

Naushad, M., Alqadami, A. A., Al-Kahtani, A. A., Ahamad, T., Awual, M. R. & Tatarchuk, T. 2019a Adsorption of textile dye using para-aminobenzoic acid modified activated carbon: kinetic and equilibrium studies. *J. Mol. Liq.* **296**, 112075. https://doi.org/10.1016/j.molliq.2019.112075.

Naushad, M., Alqadami, A. A., AlOthman, Z. A., Alsohaimi, I. H., Algamdi, M. S. & Aldawsari, A. M. 2019b Adsorption kinetics, isotherm and reusability studies for the removal of cationic dye from aqueous medium using arginine modified activated carbon. *J. Mol. Liq.* **293**, 111442. https://doi.org/10.1016/j.molliq.2019.111442.

Oguz, E., Keskinler, B. & Çelik, Z. 2005 Ozonation of aqueous Bomaplex Red CR-L dye in a semi-batch reactor. *Dye. Pigment.* **64**, 101–108. https://doi.org/10.1016/j.dyepig.2004.04.009.

Oladipo, A. A. & Gazi, M. 2014 Enhanced removal of crystal violet by low cost alginate/acid activated bentonite composite beads: optimization and modelling using non-linear regression technique. *J. Water Process Eng.* **2**, 43–52. https://doi.org/10.1016/j.jwpe.2014.04.007.

Paz, A., Carballo, J., Pérez, M. J. & Domínguez, J. M. 2017 Biological treatment of model dyes and textile wastewaters. *Chemosphere.* **181**, 168–177. https://doi.org/10.1016/j.chemosphere.2017.04.046.

Peydayesh, M. & Rahbar-Kelishami, A. 2015 Adsorption of methylene blue onto *Platanus orientalis* leaf powder: kinetic, equilibrium and thermodynamic studies. *J. Ind. Eng. Chem.* **21**, 1014–1019. https://doi.org/10.1016/j.jiec.2014.05.010.

Saffaj, N., Persin, M., Younssi, S. A., Albizane, A., Bouhria, M., Loukili, H., Dach, H. & Larbot, A. 2005 Removal of salts and dyes by low $ZnAl_2O_4$-TiO_2 ultrafiltration membrane deposited on support made from raw clay. *Sep. Purif. Technol.* **47**, 36–42. https://doi.org/10.1016/j.seppur.2005.05.012.

Sathishkumar, K., AlSalhi, M. S., Sanganyado, E., Devanesan, S., Arulprakash, A. & Rajasekar, A. 2019 Sequential electrochemical oxidation and bio-treatment of the azo dye Congo red and textile effluent. *J. Photochem. Photobiol. B Biol.* **200**, 111655. https://doi.org/10.1016/j.jphotobiol.2019.111655.

Shaim, A., Amaterz, E., Naciri, Y., Taoufyq, A., Bakiz, B., Ezahri, M., Benlhachemi, A., Ouammou, A. & Chahine, A. 2019 Synthesis, characterization and photocatalytic activity of titanophosphate glasses. *Mediterr. J. Chem.* **8** (1), mjc8119032221as. https://doi.org/10.13171/mjc8119032221as.

Sharma, G., Kumar, A., Naushad, M., García-Peñas, A., Al-Muhtaseb, A. H., Ghfar, A. A., Sharma, V., Ahamad, T. & Stadler, F. J. 2018 Fabrication and characterization of Gum arabic-cl-poly(acrylamide) nanohydrogel for effective adsorption of crystal violet dye. *Carbohydr. Polym.* **202**, 444–453. https://doi.org/10.1016/j.carbpol.2018.09.004.

Smitha, T., Santhi, T., Prasad, A. L. & Manonmani, S. 2017 *Cucumis sativus* used as adsorbent for the removal of dyes from aqueous solution. *Arab. J. Chem.* **10**, S244–S251. https://doi.org/10.1016/j.arabjc.2012.07.030.

Sulyman, M. 2014 Fixed-bed column packed with low-cost spent tea leaves for the removal of crystal violet from aqueous solution. *5th Int. Conf. Environ. Sci. Technol.*, 110–118. https://doi.org/10.7763/IPCBEE.

Tunç, Ö., Tanaci, H. & Aksu, Z. 2009 Potential use of cotton plant wastes for the removal of Remazol Black B reactive dye. *J. Hazard. Mater.* **163**, 187–198. https://doi.org/10.1016/j.jhazmat.2008.06.078.

Yagmur, E., Ozmak, M. & Aktas, Z. 2008 A novel method for production of activated carbon from waste tea by chemical activation with microwave energy. *Fuel.* **87**, 3278–3285. https://doi.org/10.1016/j.fuel.2008.05.005.

Yan, H., Li, H., Yang, H., Li, A. & Cheng, R. 2013 Removal of various cationic dyes from aqueous solutions using a kind of fully biodegradable magnetic composite microsphere. *Chem. Eng. J.* **223**, 402–411. https://doi.org/10.1016/j.cej.2013.02.113.

Yao, M., Ding, Y., Wang, Z., Deng, Y., Zhao, F., Repo, E., Yin, D., Meng, Y., Jafari, S. & Sillanpää, M. 2015 EDTA-cross-linked β-cyclodextrin: an environmentally friendly bifunctional adsorbent for simultaneous adsorption of metals and cationic dyes. *Environ. Sci. Technol.* **49**, 10570–10580.

Zhang, L., Zhang, H., Guo, W. & Tian, Y. 2014 Removal of malachite Green and crystal violet cationic dyes from aqueous solution using activated sintering process red mud. *Appl. Clay Sci.* **93–94**, 85–93. https://doi.org/10.1016/j.clay.2014.03.004.

First received 12 July 2021; accepted in revised form 24 September 2021. Available online 8 October 2021